ϕ photoproduction near threshold with Okubo-Zweig-Iizuka evading ϕNN interactions

Robert A. Williams*
Thomas Jefferson National Accelerator Facility, 12000 Jefferson Avenue, Newport News, Virginia 23606
(Received 15 September 1997)

Existing intermediate and high energy ϕ-photoproduction data is consistent with purely diffractive production (i.e., Pomeron exchange). However, near threshold ($1.574\ \text{GeV} < E_\gamma^{\text{lab}} \leqslant 2.0\ \text{GeV}$) the energy dependence of the diffractive amplitude is not well known and nondiffractive amplitudes such as π^0 and η exchange, $s\bar{s}$ knockout, and nonzero ϕNN couplings can give sizable contributions to the cross section and polarization density matrix elements of the $\phi \to K^+K^-$ decay angular distribution. We stress the importance of measurements with linearly polarized photons near the ϕ threshold to separate natural and unnatural parity exchange mechanisms. Approved and planned ϕ photoproduction and electroproduction experiments at Jefferson Lab will help establish the relative dynamical contributions near threshold and clarify outstanding theoretical issues related to apparent Okubo-Zweig-Iizuka violations. [S0556-2813(98)05201-7]

PACS number(s): 25.20.Lj, 13.60.Le, 21.30.Cb

I. INTRODUCTION

Recent observations of large ϕ production cross sections in $p\bar{p} \to \phi X$ ($X = \pi, \eta, \omega, \rho, \pi\pi, \gamma$) experiments [1] indicate a large apparent violation of the Okubo-Zweig-Iizuka (OZI) rule [2], which essentially states that couplings between states with no common quark flavors (i.e., disconnected or hairpin quark graphs) are suppressed. In the naive quark model, the proton has no $s\bar{s}$ content whereas the ϕ meson is an ideally mixed, pure $s\bar{s}$ state, and thus the OZI rule predicts negligible ϕNN couplings and permits only strange hadronic decays of the ϕ (such as $\phi \to K^+K^-$). Actually, the nonstrange $\phi \to \rho\pi$ decay has a 13% branching ratio which is much larger than naively expected from the OZI rule. However, it is incorrect to interpret this decay as an OZI violation since there are two distinct mechanisms which permit connected quark loops and hence a nonstrange decay without violating the OZI rule. The first possibility involves two-step OZI allowed final state interactions such as $\phi \to K\bar{K} \to \rho\pi$. A second possibility follows from the realization that the ϕ meson is not simply a pure $s\bar{s}$ state. The ϕ actually has a small $u\bar{u} + d\bar{d}$ component which can couple to the nonstrange $\rho\pi$ decay channel without violating the OZI rule. These two possibilities show that a distinction should be made between couplings (or decays) that actually violate the OZI rule and those which *evade* the OZI rule through final state interactions or intrinsic flavor wave function components beyond the naive quark model assignments. To reiterate, the terminology OZI evasion applies to couplings such as $\phi \to \rho\pi$ where the OZI rule does not strictly apply since connected quark graphs exist. Obviously, the apparent OZI ''violations'' observed in $p\bar{p} \to \phi X$ can be interpreted as a manifestation of OZI evasion if the nucleon wave function contains an explicit $s\bar{s}$ (hidden strangeness) component or strong final state interactions mediate ϕ production.

In this paper, we present a quantum hadrodynamical (QHD) model calculation for ϕ photoproduction with a focus on sensitivity to nondiffractive production mechanisms near threshold (including OZI evading interactions). To help motivate this analysis, a review of the broad based experimental, phenomenological, and theoretical work on OZI evasion is presented in the next section. In Sec. II, we present a general discussion of the nondiffractive mechanisms expected to contribute to ϕ photoproduction near threshold. The importance of using linearly polarized photons and measuring the full $\phi \to K^+K^-$ decay angular distribution is emphasized in Sec. III. We present details of our QHD model in Sec. IV, discuss numerical results in Sec. V, and summarize conclusions in Sec. VI.

II. OZI EVADING MECHANISMS

In the recent data which indicate large apparent OZI violations, there is a notable spin, channel, and momentum transfer dependence. For example, (i) the $\phi\pi$ and $\phi\gamma$ channels exhibit strong enhancement over the OZI prediction, whereas much smaller deviations are observed in other channels; (ii) the apparent OZI violation for small momentum transfer (e.g., $p\bar{p}$ at rest) is much larger than at higher energies; (iii) the enhancement of the $\phi\pi^0$ channel appears only from S-wave $p\bar{p}$ annihilation with no observed OZI violation in the P wave.

Several calculations have explored the possibility that the apparent OZI violations result from strong final state interactions mediated by OZI allowed two-step mechanisms involving $K\bar{K}$, $K^*\bar{K} + \bar{K}^*K$, $K\bar{K}\pi\pi$, and $\Lambda\bar{\Lambda}$ intermediate states [3–9]. These calculations share the virtue of using experimentally known cross sections and branching ratios which tightly constrain the amplitudes of various subprocesses driving the OZI evasion. A primary criticism of this approach is that strong cancellations are possible (and in some cases expected) between different hadronic loops [10,11], and hence calculations employing a truncated set of

*Present address: Hampton University, Department of Physics, Hampton Virginia, 23668. Electronic address: bobw@cebaf.gov

intermediate states can at best provide an upper limit to the OZI evasion [12]. However, these two-step calculations do obtain the right order of magnitude for the observed OZI evasion in all of the various channels. We note that the observed dependence of OZI evasion on the initial spin and orbital state of the $p\bar{p}\to\phi\pi^0$ reaction provides an interesting possibility for testing the consistency of the two step scenario. As pointed out in Refs. [8,12], measurements would be useful to verify whether or not the isospin $I=1$ amplitude of the $p\bar{p}\to K^*\bar{K}+\bar{K}^*K$ reaction is substantially larger for S-wave $^3S_1(p\bar{p})$ annihilation compared with P-wave $^1P_1(p\bar{p})$ annihilation. If not, then the observed excess in $p\bar{p}\to\phi\pi^0$ from S-wave annihilation would be difficult to explain from strong final state interactions. Buzatu and Lev [13] have clarified this point by demonstrating that since $\phi\pi^0$ can be produced with $l=0,2$ in the P-wave annihilation channel, there is a possibility that large destructive interference between the $l=0$ and $l=2$ amplitudes could account for the unobserved OZI evasion in this channel even if the $K^*\bar{K}+\bar{K}^*K$ production amplitudes are comparable for S-wave and P-wave annihilation. This possibility seems unlikely, however a measurement of the $K^*\bar{K}$ ($\bar{K}^*K$) angular distribution in P-wave $p\bar{p}$ annihilation can (in principle) resolve this issue and provide a decisive test of the two-step mechanism.

Dover and Fishbane have suggested that the existence of a $J^{PC}=1^{--}$ $\phi\pi$ resonance [the ''$C(1480)$ meson''] may be responsible for enhanced ϕ production in certain $p\bar{p}$ annihilation channels [14]. This resonance can naturally provide enhanced $\phi\pi^0$ production in S-wave annihilation while decoupling from P-wave annihilation. Unfortunately, no deviations from the OZI rule have been observed in the $\phi\eta$ channel where the predicted isoscalar partner of the C meson should couple strongly. Furthermore, the C meson is not well established and it is not a resonance in the $\phi\gamma$ channel where the largest OZI evasion is observed. It is clear that the C-meson resonance can not explain all of the observed OZI deviations, but it is nonetheless an interesting, albeit controversial possibility in the $\phi\pi^0$ channel.

Ellis *et al.* suggest that the pattern of observed OZI evasion is difficult to understand without preexisting strangeness in the nucleon [12,15] (see Ref. [16] for a critical review). Allowing for intrinsic hidden strangeness, the nucleon wave function is generically expressed:

$$|p\rangle = A|uud\rangle + B|uud\otimes(s\bar{s})\rangle. \tag{1}$$

Using this ansatz, Ellis *et al.* showed that the apparent OZI violating features (i),(ii),(iii) can be explained by (OZI evading) strangeness ''knockout'' and ''rearrangement'' mechanisms with a nucleon strangeness admixture probability in the range $0.01\leqslant|B|^2\leqslant 0.19$. This estimate is consistent with the analyses of other independent experimental results such as the EMC deep inelastic μp scattering [17], BNL elastic νp scattering [18], and measurements of the πN sigma term [19] which consistently find a strangeness admixture of approximately $10-20\,\%$. For electromagnetic ϕ production, the knockout mechanism has been shown to yield a substantial contribution to the cross section with a moderate strangeness admixture. For example, Henley *et al.* [20] used a nonrelativistic constituent quark model to calculate ϕ photoproduction and electroproduction from the proton with intrinsic strangeness and estimated an upper limit for $|B|^2 \sim 10-20\,\%$. Recently, Titov *et al.* [21] have explored a relativistic (covariant oscillator) quark model showing that with less than 5% admixture of strange quarks in the proton the ϕ photoproduction cross section from $s\bar{s}$ knockout is comparable to diffractive production. Furthermore, Titov *et al.* showed that the beam-target (BT) and beam-recoil (BR) double polarization observables are particularly sensitive to the hidden strangeness component. We note that the quark model calcuations discussed here were not constrained by the nucleon mass or other properties (e.g., magnetic moments, form factors) which we expect could place strong restrictions on the allowable range for hidden strangeness components.

Assuming the viability of the hidden strangeness hypothesis, another direct consequence is the affect on electromagnetic properties such as nucleon magnetic moments and form factors. Recent lattice QCD calculations have found evidence that intrinsic strangeness is essential for understanding the magnetic moments of the octet baryons, with 11% of the proton's magnetic moment coming from strange quarks [22]. Consistent with this finding are vector meson dominance (VMD) and dispersion relation models of the electromagnetic nucleon form factors. These models employ effective OZI evading $g^{V,T}_{\phi NN}$ vector and tensor couplings which strongly affect the isoscalar nucleon form factors. For example, OZI evading ϕNN couplings contribute to the nucleon strangeness radius, strange magnetic moment, and have been shown to provide a significant improvement to fits of $G^n_E(q^2)$ [23–27].

An OZI evading QHD interaction Lagrangian (with $g^{V,T}_{\phi NN}$ couplings) provides a complementary parametrization of the strange quark knockout and loop order effects. For example, in the simplest quark model realization of Eq. (1) the $s\bar{s}$ pairs in the nucleon form a color singlet cluster that couple to spin 0 or 1 (in a relative P wave with respect to the nonstrange cluster) [21]. The spin 0 component has the quantum numbers of an intrinsic η_s (i.e., strange component of η meson) whereas the spin 1 component has intrinsic ϕ meson quantum numbers. In principle, the QHD ϕNN couplings can be related to underlying quark dynamics through overlap matrix elements of quark model wave functions with an intrinsic ϕ-cluster component. Similarly, an intrinsic η_s component of the nucleon will give a dynamical contribution to the effective value of the ηNN coupling constant. Even without intrinsic nucleon strangeness, effective ϕNN couplings absorb dynamical contributions from hadronic loops with OZI conserving meson-baryon interactions. Explicit constituent quark model [11] and QHD [28] loop order calculations of the nucleon strangeness radius and magnetic moment using well constrained OZI conserving interactions have shown large cancellations between loops, implying very small effective ϕNN couplings (consistent with OZI suppression). These results suggest that evidence for anomolously large ϕNN couplings would represent a phenomenological manifestation of intrinsic nucleon strangeness.

For the sake of this study, we treat the $g^{V,T}_{\phi NN}$ and $g_{\eta NN}$ couplings as unconstrained parameters which we adjust to fit the existing ϕ photoproduction data. With a phenomenological treatment such as this, we realize the ϕNN couplings are only effective constants which parametrize the OZI evading interactions (two-step loops and/or hidden strangeness) occurring at a more fundamental level. A primary focus of this work is to test whether the cross section or polarization observables measured from the $\phi \to K^+K^-$ decay angular distribution are sensitive to the ϕNN and ηNN couplings.

III. NONDIFFRACTIVE ϕ-PRODUCTION MECHANISMS

There are several possible mechanisms which can contribute to observable deviations from diffractive ϕ photoproduction. For example, an approved Jefferson Lab experiment will be focusing on two-gluon exchange interference in ϕ production in the large-t region [29]. This two-gluon mechanism respects s-channel helicity conservation (SCHC) and can be separated from other t-channel mechanisms (e.g., pseudoscalar exchange and strangeness knockout) in an experiment using linearly polarized photons (discussed in the next section). In addition to the strangeness knockout, two-step, and effective ϕNN interactions discussed in the previous section, pseudoscalar π^0 and η meson exchange amplitudes are expected to be non-negligible with maximum contributions at low energy near the ϕ production threshold. Recent model calculations have shown that for $W \approx 2.0$ GeV these unnatural parity amplitudes can be comparable or larger than diffractive production via Pomeron exchange [30]. The effective couplings of the π exchange amplitude are relatively well known (e.g., $g_{\pi NN}$ and $\mu_{\phi\pi\gamma}$), however, the ηNN coupling is uncertain and its value can be another measure of the intrinsic nucleon strangeness content. Specifically, the ηNN coupling can be related to the axial flavor singlet nucleon charge through the $U_A(1)$ anomaly in QCD. Hatsuda has shown that the ηNN coupling should be suppressed relative to the naive SU(3) prediction to be consistent with the EMC data [31]. A phenomenological study of low energy η photoproduction indeed found a suppressed ηNN coupling, but contradicts the Bonn potential which gives enhancement relative to SU(3) [32]. Our results confirm that precision ϕ photoproduction data near threshold will provide sensitive constraints on the ηNN coupling. We neglect contributions from η' exchange due to its relatively large mass (giving propagator suppression) and highly uncertain hadronic and electromagnetic couplings.

One additional (speculative) nondiffractive mechanism for ϕ photoproduction is worth noting. Recently, two very narrow baryon resonances were observed in $p + {}^{12}\mathrm{C}$ reactions which decay dominantly into strange channels [33]. These states, called the $X(2000)$ and $X(2050)$, have been interpreted as five-quark, color octet, or sextet bonded exotic baryons containing $s\bar{s}$ pairs [34], or possibly molecular ϕN or K^*Y ($Y = \Lambda, \Sigma$) resonances [35]. Strange baryon resonances permit an OZI allowed strong decay in the ϕp channel, and consequently these novel states may produce interesting resonance enhancement and/or interference effects just above the ϕ photoproduction threshold.

IV. IMPORTANCE OF LINEARLY POLARIZED PHOTONS AND $\phi \to K^+K^-$ ANGULAR DISTRIBUTION

A primary advantage of ϕ production measurements using a 4π acceptance spectrometer (such as the Hall B CLAS at Jefferson Lab) is that the full angular distribution of the vector ϕ decay can be measured which gives information about the polarization state of the ϕ prior to decay, in addition to the differential cross section. Quantitatively, the ϕ meson decay angular distribution gives information about independent bilinear combinations of the helicity amplitudes (polarization density matrices). For ϕ photoproduction with linearly polarized photons, the full decay angular distribution can be expressed [36]:

$$W_L(\theta,\phi,\Phi) = W^0(\theta,\phi) - P_\gamma \cos 2\Phi\, W^1(\theta,\phi) - P_\gamma \sin 2\Phi\, W^2(\theta,\phi), \tag{2}$$

where P_γ is the degree of linear polarization of the photon, Φ is the angle between the photon polarization direction and the ϕ-production plane, and (θ,ϕ) are the polar and azmuthal angles of the K^+K^- pairs in the helicity (H) frame, defined as the ϕ rest frame with z-direction taken opposite to the recoil proton in the c.m. system. The normalized $W^j(\theta,\phi)$ $(j = 0,1,2)$ functions are expressed in terms of the polarization density matrix elements $\rho^\alpha_{\lambda\lambda'}$:

$$W^0(\theta,\phi) = \frac{3}{4\pi}\left[\frac{1}{2}(1-\rho^0_{00}) + \frac{1}{2}(3\rho^0_{00}-1)\cos^2\theta - \sqrt{2}\,\mathrm{Re}[\rho^0_{10}]\sin 2\theta\cos\phi - \rho^0_{1-1}\sin^2\theta\cos 2\phi\right], \tag{3}$$

$$W^1(\theta,\phi) = \frac{3}{4\pi}[\rho^1_{11}\sin^2\theta + \rho^1_{00}\cos^2\theta - \sqrt{2}\rho^1_{10}\sin 2\theta\cos\phi - \rho^1_{1-1}\sin^2\theta\cos 2\phi], \tag{4}$$

$$W^2(\theta,\phi) = \frac{3}{4\pi}[\sqrt{2}\,\mathrm{Im}[\rho^2_{10}]\sin 2\theta\cos\phi - \mathrm{Im}[\rho^2_{1-1}]\sin^2\theta\cos 2\phi]. \tag{5}$$

The $W^0(\theta,\phi)$ function is the distribution for the ϕ decay from unpolarized photons whereas the $W^{1,2}(\theta,\phi)$ functions correspond to the extra terms associated with two independent linear polarization orientations of the photon. We write the expressions for the $\rho^\alpha_{\lambda\lambda'}$ matrix elements in terms of helicity amplitudes in the next section.

Two features of photoproduction with linearly polarized photons are worth noting. Compared with any other photoproduction polarization observable, using a linearly polarized photon source with subsequent detection of the ϕ decay distribution provides access to the maximum number of independent density matrix elements (nine elements, compared with five for circularly polarized and three for unpolarized photons). Another key advantage of using linearly polarized photons is that seven of the nine measurable density matrix elements can be separated into contributions from natural and unnatural parity exchanges in the t channel, whereas

experiments with unpolarized or circularly polarized photons do not yield any information on the nature of the t-channel exchanges [36]. Since unnatural parity exchange amplitudes violate SCHC, separation of the t-channel parity matrix elements will prove to be extremely useful for disentangling the competing dynamical mechanisms present in ϕ photoproduction near threshold. An extra benefit of measuring the complete angular distribution of K^+K^- production is the possibility to resolve interference between the P-wave ϕ decay component and S-wave K^+K^- pairs which couple strongly to the $f_0(980)$ and $a_0(980)$ scalar meson resonances [37]. The scalar mesons have controversial quark (exotic), gluonic (hybrid), and/or molecular structure, thus ϕ photoproduction can provide valuable indirect information about these novel states.

V. QHD MODEL DETAILS

To establish notation we specify the ϕ photoproduction reaction

$$\gamma(q,h_\gamma)+p(p,\sigma)\rightarrow\phi(k,h_\phi)+p(p',\sigma'), \tag{6}$$

where the energy-momentum four-vectors for the photon, initial proton, ϕ, and recoil proton are given by q, p, k, and p', respectively. The photon (ϕ) helicity is denoted by h_γ (h_ϕ), and the initial (final) proton spin is labeled by σ (σ'). The photoproduction helicity amplitudes ($T_{h_\phi\sigma' h_\gamma\sigma}$) can be expressed:

$$T_{h_\phi\sigma' h_\gamma\sigma}\equiv\epsilon_\mu(h_\gamma)\phi^*_\nu(h_\phi)\mathcal{H}^{\mu\nu}_{\sigma'\sigma}, \tag{7}$$

where $\epsilon_\mu(h_\gamma)$ and $\phi_\nu(h_\phi)$ are the photon and ϕ polarization four-vectors in the helicity basis, respectively, and $\mathcal{H}^{\mu\nu}_{\sigma'\sigma}$ is the hadronic current tensor obtained by application of Feynman rules to the tree level QHD diagrams. We evaluate the hadronic current tensor in the Gottfried-Jackson (GJ) system, defined as the ϕ meson rest frame with the z axis taken to be in the direction of the incoming photon. The GJ frame is a ''characteristic frame'' of t-channel processes since in this frame the polarization density matrix elements of t-channel exchanges are independent of both energy and production angle. In the GJ frame, the photon and ϕ polarization four-vectors have the same form for the transverse (helicity $\pm$) components

$$\phi_\mu(\lambda)=\epsilon_\mu(\lambda)=-\frac{\lambda}{\sqrt{2}}(0,1,i\lambda,0)\quad(\lambda=\pm), \tag{8}$$

$$\phi_\mu(\lambda)=(0,0,0,1)\quad(\lambda=0). \tag{9}$$

The density matrix elements are computed from the helicity amplitudes through the relations

$$\rho^0_{\lambda\lambda'}=\frac{1}{2N}\sum_{h_\gamma\sigma'\sigma}T_{\lambda\sigma' h_\gamma\sigma}T^*_{\lambda'\sigma' h_\gamma\sigma}, \tag{10}$$

$$\rho^1_{\lambda\lambda'}=\frac{1}{2N}\sum_{h_\gamma\sigma'\sigma}T_{\lambda\sigma'-h_\gamma\sigma}T^*_{\lambda'\sigma' h_\gamma\sigma}, \tag{11}$$

$$\rho^2_{\lambda\lambda'}=\frac{i}{2N}\sum_{h_\gamma\sigma'\sigma}h_\gamma T_{\lambda\sigma' h_\gamma\sigma}T^*_{\lambda'\sigma' h_\gamma\sigma}, \tag{12}$$

where N is the normalization factor related to the unpolarized differential cross section

$$N=\frac{1}{2}\sum_{\lambda h_\gamma\sigma'\sigma}|T_{\lambda\sigma' h_\gamma\sigma}|^2,\quad\frac{d\sigma}{dt}=\frac{M_p^2(\hbar c)^2}{32\pi s|\mathbf{q}_{\rm c.m.}|^2}N. \tag{13}$$

The GJ density matrix elements can be transformed into the helicity (H) frame appropriate for Eqs. (2)–(5) by multiplication with the Wigner rotation functions $\rho(H)=D^1(\psi,0)\rho(\mathrm{GJ})D^1(\psi,0)^\dagger$, where ψ is the angle between the photon direction in the ϕ rest frame and the ϕ momentum direction in the total c.m. system. Explicitly, in terms of the c.m. momenta ($|\mathbf{q}|$ and $|\mathbf{k}|$) and the ϕ production angle Θ:

$$\cos\psi=\frac{\mathbf{k}\cdot(\mathbf{q}-\mathbf{k})}{|\mathbf{k}||\mathbf{q}-\mathbf{k}|}=\frac{|\mathbf{q}|\cos\Theta-|\mathbf{k}|}{[|\mathbf{q}|^2+|\mathbf{k}|^2-2|\mathbf{q}||\mathbf{k}|\cos\Theta]^{1/2}}. \tag{14}$$

The effective QHD Lagrangian densities for the strong and electromagnetic interactions are implied by the following expressions for individual contributions to the hadronic current tensor.

t-channel 0^+ *Pomeron* ($\mathcal{P}$) *exchange.*

$$\mathcal{H}^{\mu\nu}_{\sigma'\sigma}=\frac{eG_{\mathcal{P}}}{M_\phi}\Pi_{\mathcal{P}}(t)\left(\frac{s-s_{th}}{s_0}\right)^{\alpha(t)}\overline{u}(p',\sigma')u(p,\sigma)\times[q\cdot k g^{\mu\nu}-k^\mu q^\nu]. \tag{15}$$

t-channel 0^- *meson exchange* ($x=\pi^0,\eta$).

$$\mathcal{H}^{\mu\nu}_{\sigma'\sigma}=\frac{e\kappa_{\phi\gamma x}g_{xNN}F_t(t;\lambda)}{M_\phi[(p'-p)^2-M_x^2]}\overline{u}(p',\sigma')\gamma_5u(p,\sigma)\epsilon^{\mu\alpha\nu\beta}q_\alpha k_\beta. \tag{16}$$

OZI evading s channel.

$$\mathcal{H}^{\mu\nu}_{\sigma'\sigma}=eg^V_{\phi NN}F_s(s;\lambda)\overline{u}(p',\sigma')\left[\gamma^\nu+\frac{i\kappa^T_\phi}{2M_p}\sigma^{\nu\alpha}k_\alpha\right]\times\frac{(p+q)\cdot\gamma+M_p}{(p+q)^2-M_p^2}\left[\gamma^\mu+\frac{i\kappa^T_p}{2M_p}\sigma^{\mu\beta}q_\beta\right]u(p,\sigma). \tag{17}$$

OZI evading u channel.

$$\mathcal{H}^{\mu\nu}_{\sigma'\sigma}=eg^V_{\phi NN}F_u(u;\lambda)\overline{u}(p',\sigma')\left[\gamma^\mu+\frac{i\kappa^T_p}{2M_p}\sigma^{\mu\beta}q_\beta\right]\times\frac{(p'-q)\cdot\gamma+M_p}{(p'-q)^2-M_p^2}\left[\gamma^\nu+\frac{i\kappa^T_\phi}{2M_p}\sigma^{\nu\alpha}k_\alpha\right]u(p,\sigma). \tag{18}$$

Note that the Pomeron exchange amplitude is coupled to the nucleon and ϕ meson with scalar (0^+) quantum numbers [i.e., $\overline{u}(p',\sigma')u(p,\sigma)$ for the $\mathcal{P}$-nucleon coupling and

TABLE I. Pomeron parameters of model I (Regge propagator, $s_{\rm th}=s_0$) and model II [Empirical propagator with (a) $s_{\rm th}=0$, (b) $s_{\rm th}=s_0$]. Unadjusted parameter: (Pomeron pole mass) $M_{\mathcal{P}}=1.3$ GeV. Note the sensitivity to the Pomeron Regge intercept α_0 in model I (implied by significant figures displayed). The Pomeron intercept of model II(a) violates the Froissart limit $\alpha_0\leq 1$ and thus produces an unphysical high energy behavior.

	$G_{\mathcal{P}}$	α_0	$\alpha'(\mathrm{GeV}^{-2})$	$\beta(\mathrm{GeV}^{-2})$
Model I	1.6	0.962	0.25	
Model II(a)	8.5	1.25	0.27	3.0
Model II(b)	17.0	1.0	0.27	3.0

TABLE II. Lagrangian parameters of model I (Regge propagator, $s_{\rm th}=s_0$) and model II [Empirical propagator with (a) $s_{\rm th}=0$, (b) $s_{\rm th}=s_0$]. Unadjusted parameters: (anomalous tensor coupling of the proton) $\kappa_p^T=1.793$, (psuedoscalar πNN coupling) $g_{\pi NN}=13.8$, (form factor cutoff) $\lambda=0.5$ GeV. The magnitudes of the radiative ϕ decay constants are determined by the experimental partial widths.

	$g_{\eta NN}$	$g^V_{\phi NN}$	κ^T_ϕ	$\kappa_{\phi\gamma\pi}$	$\kappa_{\phi\gamma\eta}$
Model I	6.3	-0.3	0.33	0.143	0.708
Model II(a)	2.6	-0.8	0.13	0.143	-0.708
Model II(b)	7.3	-0.7	0.0	0.143	0.708

$F^{\gamma}_{\mu\nu}F^{\mu\nu}_{\phi}$ for the $\mathcal{P}$-γ-ϕ coupling] with a dimensionless strength $G_{\mathcal{P}}$, and has asymptotic energy dependence consistent with Regge theory $(s/s_0)^{\alpha(t)}$ [38]. The Pomeron Regge trajectory is parametrized by the conventional linear form $\alpha(t)=\alpha_0+\alpha' t$. We note that Regge theory only establishes the asymptotic high energy behavior of the diffractive amplitude, and since the energy dependence of the diffractive amplitude is poorly known at low energy, we introduce a parameter $s_{\rm th}$ $(0\leq s_{\rm th}\leq s_0)$ which governs the relative strength of diffractive production near threshold. We take the reference energy $(\sqrt{s_0})$ to be fixed at threshold, $s_0=(M_\phi+M_p)^2$. $\Pi_{\mathcal{P}}(t)$ is an effective Pomeron propagator which is parametrized in two distinct model prescriptions.

Model I (Regge theory):

$$\Pi_{\mathcal{P}}(t)=\frac{1}{2}(1-e^{-i\pi\alpha(t)})\frac{\pi\alpha'}{\sin[\pi\alpha(t)]}\frac{1}{\Gamma[1+\alpha(t)]}. \quad (19)$$

Model II (empirical):

$$\Pi_{\mathcal{P}}(t)=\frac{e^{\beta t}}{t-M^2_{\mathcal{P}}}. \quad (20)$$

In model II, a perturbative scalar meson propagator with a pole mass fixed at $M_{\mathcal{P}}=1.3$ GeV (appropriate for the lightest scalar glueball candidate or f_0 exchange) is modified by an empirical exponential factor $(e^{\beta t})$, which reproduces the observed t dependence of the diffractive cross section.

We investigate two extreme cases for the threshold parameter $(s_{\rm th})$ corresponding to versions (a) (with $s_{\rm th}=0$), and (b) (with $s_{\rm th}=s_0$) of model II. In the model I (Regge) prescription, the available data strongly selects the maximum value for the threshold parameter $s_{\rm th}\to s_0$, hence we present only one version of model I with $s_{\rm th}=s_0$. The purpose of introducing two Pomeron propagator prescriptions and investigating two versions of the diffractive threshold energy dependence is to test the stability and sensitivity of the ϕNN and ηNN coupling constants to different assumptions about the diffractive component of the amplitude.

In each of the t-, s-, and u-channel amplitudes, Eqs. (16)–(18), we employ a hadronic interaction cutoff function to account for the composite structure of the nucleon and mesons. The hadronic form factors can be calculated in constituent quark models and have been shown to be very important in regulating the energy and momentum transfer dependence in meson photoproduction [39,40]. However, to preserve the covariance and crossing properties of our model we employ phenomenological form factors:

$$F_x(x;\lambda)=\frac{\lambda^4+x^2_{\rm min}}{\lambda^4+x^2} \quad (x=s,t,u), \quad (21)$$

where ''x'' is dummy for the appropriate Mandelstam variable in each channel. The form factors are normalized to

TABLE III. Model predictions for the measurable density matrix elements in the GJ frame ($0\leq a,c,e\leq 1$, $-1/2\leq b,d,f,g\leq +1/2$).

	0^+	gg	0^-	$(s\bar{s})_0$	$(s\bar{s})_1$	ϕNN	All
ρ^0_{11}	1/2	1/2	1/2	1/2	$\frac{1}{2}(1-\mathbf{a})$	$\frac{1}{2}(1-\mathbf{c})$	$\frac{1}{2}(1-\mathbf{e})$
ρ^0_{10}	0	0	0	0	$\neq 0$	$\neq 0$	$\neq 0$
ρ^0_{1-1}	0	0	0	0	$\neq 0$	$\neq 0$	$\neq 0$
ρ^0_{00}	0	0	0	0	**a**	**c**	**e**
ρ^1_{11}	0	0	0	0	$\neq 0$	$\neq 0$	$\neq 0$
ρ^1_{10}	0	0	0	0	$\neq 0$	$\neq 0$	$\neq 0$
ρ^1_{1-1}	$+1/2$	$+1/2$	$-1/2$	$-1/2$	**b**	**d**	**f**
ρ^1_{00}	0	0	0	0	$\neq 0$	$\neq 0$	$\neq 0$
ρ^2_{10}	0	0	0	0	$\neq 0$	$\neq 0$	$\neq 0$
ρ^2_{1-1}	$-i/2$	$-i/2$	$+i/2$	$+i/2$	$-i$**b**	$-i$**d**	i**g**

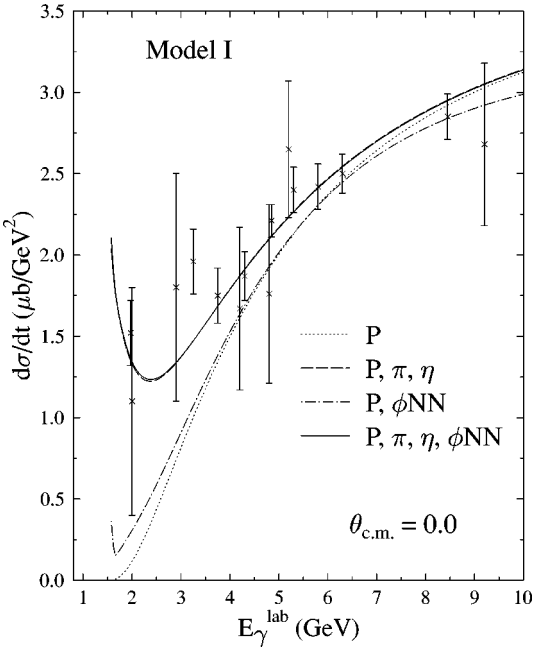

FIG. 1. Threshold energy dependence of model I differential cross section at $t_{\min}$. Different curves represent results with amplitude combinations as labeled in the key. Data is from a compilation of references in [41].

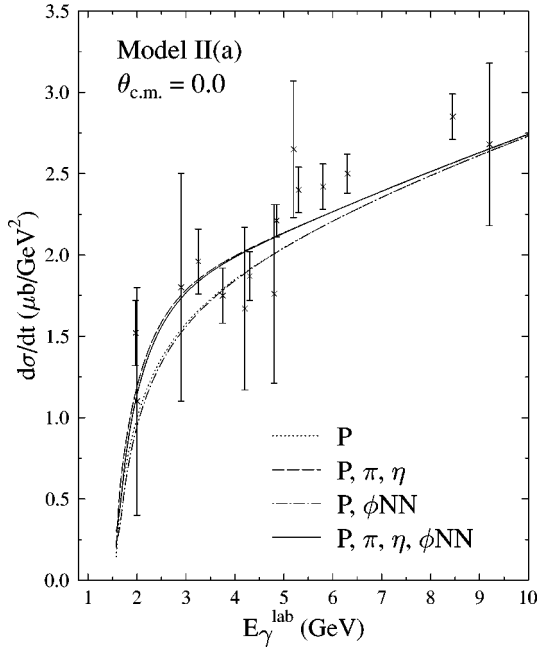

FIG. 2. Threshold energy dependence of model II(a) differential cross section at $t_{\min}$ showing results from different amplitude combinations.

unity at $s_{\min}=s_0$ (threshold), $t_{\min}=t(\Theta^{\text{c.m.}}_{\gamma\phi}=0)$, and $u_{\min}=u(\Theta^{\text{c.m.}}_{\gamma\phi}=\pi)$. We assume the same value for the cutoff parameter in all channels.

All parameters are adjusted to fit the existing ϕ photoproduction data, except for $g_{\pi NN}$, the radiative decay constants $|\kappa_{\phi\gamma\pi}|$ and $|\kappa_{\phi\gamma\eta}|$ (relative phases are fit to data), and the form factor cutoff which is arbitrarily fixed at $\lambda=0.5$ GeV. We discuss sensitivity to the cutoff parameter in the numerical results section. We display the model parameters for the Pomeron amplitude in Table I and the Lagrangian parameters in Table II.

It is interesting to see the contributions of individual processes to the observable density matrix elements. We present a summary of the previously discussed dynamical processes and their corresponding measurable GJ density matrix elements in Table III. Columns 1–7 show the predictions for scalar Pomeron exchange (0^+), two-gluon (gg), pseudoscalar π and η (0^-), spin-0 strangeness knockout $[(s\bar{s})_0]$, spin-1 strangeness knockout $[(s\bar{s})_1]$, OZI evading s- and u-channel QHD amplitudes (ϕNN), and all processes combined (all) respectively. Note that the two-gluon exchange preserves SCHC and gives the same matrix elements as 0^+ exchange [29]. Similarly, the spin-0 strangeness knockout mechanism couples the photon to the intrinsic η_s component of the nucleon, having the same quantum numbers (helicity dependence) as 0^- exchange and thus contributes to the same matrix elements. The spin-1 strangeness knockout (i.e., intrinsic ϕ) and OZI evading ϕNN amplitudes do not have a characteristic frame, hence they can contribute to all density matrix elements (which are generally energy and angular dependent). Even without strangeness knockout or OZI evading QHD interactions the nonzero matrix elements in columns 1–4 can be energy and angular dependent as the relative contributions from natural parity (0^+ Pomeron) and unnatural parity (0^- π and η) exchange amplitudes are modulated. The last column of Table III shows that every matrix element is potentially nonzero when all processes contribute to ϕ production. At $\Theta_{\text{c.m.}}=0°$ (or $t_{\min}$) only the highlighted matrix elements (a,b,c,d,e,f,g) are nonzero. We note that the ρ^0_{00} matrix element is particularly interesting since it is identically zero for the conventional (Pomeron and pseudoscalar) t-channel exchange amplitudes, whereas nonzero values are generated in proportion to the spin-1 strangeness knockout and/or ϕNN amplitude component. We have confirmed numerically that compared with all other matrix elements, ρ^0_{00} has the largest sensitivity to ϕNN couplings.

Another very interesting observable is the photon polarization asymmetry, Σ defined

$$\Sigma=\frac{\sigma_\parallel-\sigma_\perp}{\sigma_\parallel+\sigma_\perp}=\frac{1}{P_\gamma}\frac{W_L(0,\pi/2,\pi/2)-W_L(0,\pi/2,0)}{W_L(0,\pi/2,\pi/2)+W_L(0,\pi/2,0)}$$
$$=\frac{\rho^1_{11}+\rho^1_{1-1}}{\rho^0_{11}+\rho^0_{1-1}}, \tag{22}$$

which essentially measures the degree of SCHC. Note the extreme limits for Σ corresponding to purely diffractive/natural parity production compared with purely nondiffractive/unnatural parity production:

$$\Sigma\rightarrow+1:\ \ 0^+\ \text{exchange},$$

$$\rightarrow-1:\ \ 0^-\ \text{exchange}.$$

Obviously, Σ is particularly sensitive to the relative strength of natural and unnatural parity exchange amplitudes, and precise measurements of Σ near threshold would be very useful for quantifying the η exchange contribution.

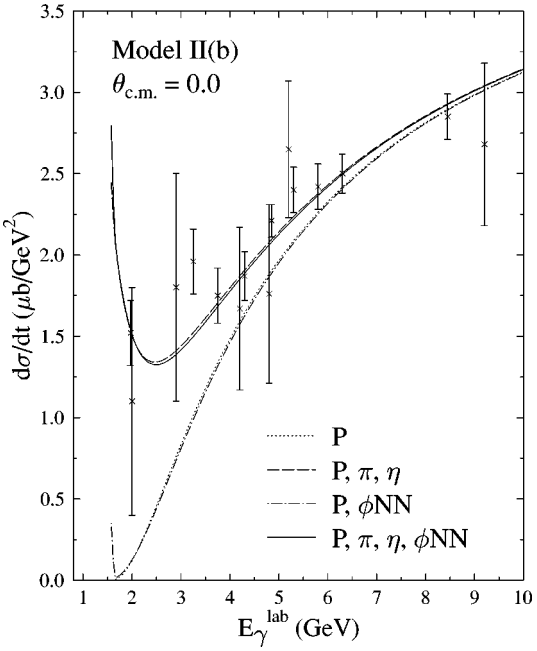

FIG. 3. Threshold energy dependence of model II(b) differential cross section at t_{min} showing results from different amplitude combinations.

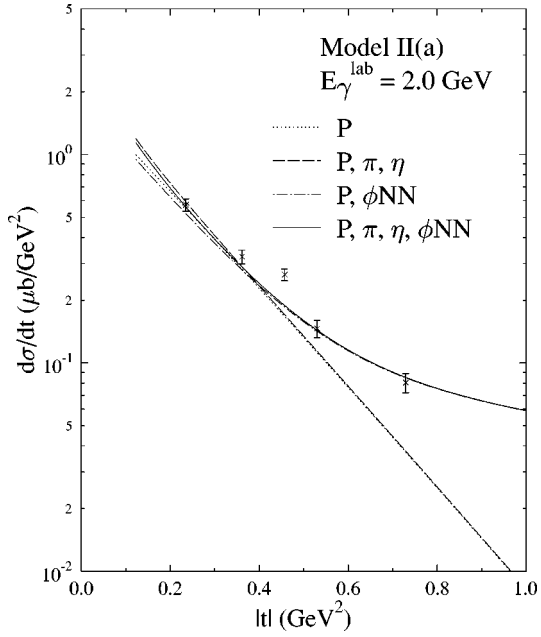

FIG. 5. Model II(a) differential cross section t dependence near threshold, showing results from different amplitude combinations.

VI. NUMERICAL RESULTS

Figures 1, 2, and 3 show the threshold energy dependence of models I, II(a), and II(b) differential cross sections respectively at t_{min} with curves showing various combinations of amplitudes (as labeled on figure). For all figures presented, the data is taken from Ref. [41] and/or references therein. Model II(a) shows little sensitivity to nondiffractive amplitudes, but models I and II(b) (by definition) have a vanishing diffractive amplitude at threshold, hence they demonstrate enhanced sensitivity to the magnitude and relative phase of nondiffractive amplitudes, especially η exchange. In all models presented and for all observables, the π exchange contribution is suppressed relative to the η since $|\kappa_{\phi\gamma\pi}| \ll |\kappa_{\phi\gamma\eta}|$. All models show very little sensitivity to the OZI evading s- and u-channel ϕNN amplitudes at t_{min}. The enhancement of the cross section seen in models I and II(b) exactly at threshold is dominantly due to the η exchange amplitude and is therefore a measure of $g^2_{\eta NN}$.

Figures 4, 5, and 6 show the t dependence of the low energy cross section data ($E_\gamma^{lab} = 2.0$ GeV) for models I, II(a), and II(b), respectively, with specific amplitude combinations displayed. The model I and II(b) results show that the dif-

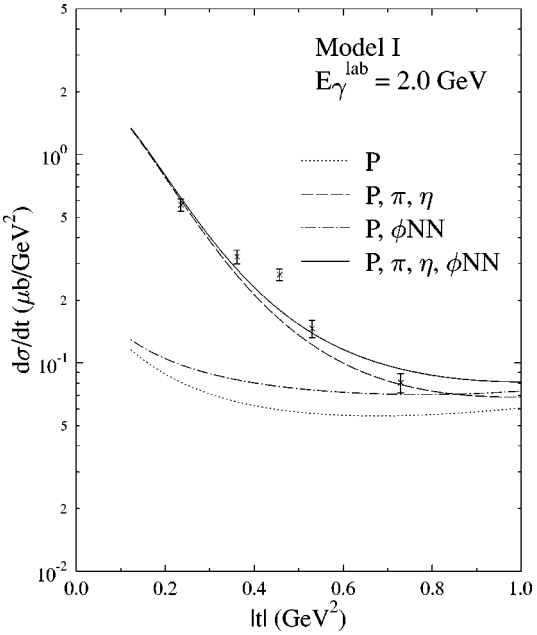

FIG. 4. Model I differential cross section t dependence near threshold, showing results from different amplitude combinations.

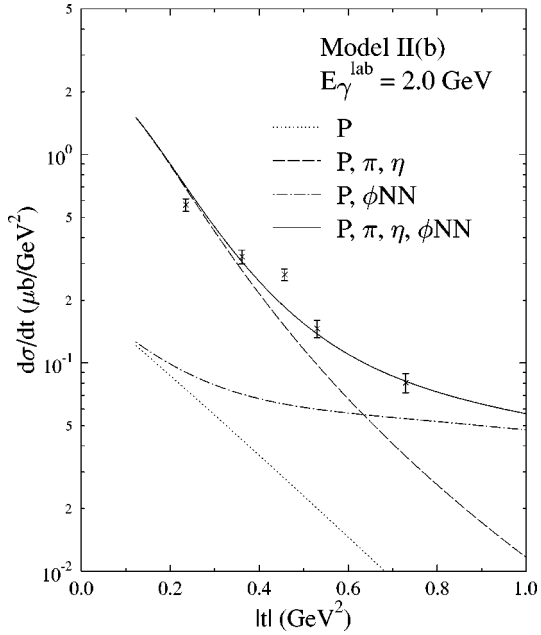

FIG. 6. Model II(b) differential cross section t dependence near threshold, showing results from different amplitude combinations.

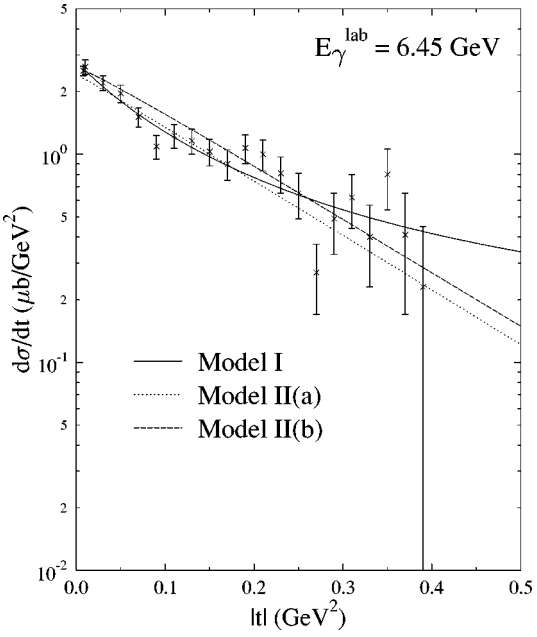

FIG. 7. Differential cross section t dependence for models I, II(a), and II(b) at higher energy, $E_\gamma^{\rm lab}=6.45$ GeV. For the t range covered by the data, nondiffractive amplitude components are small.

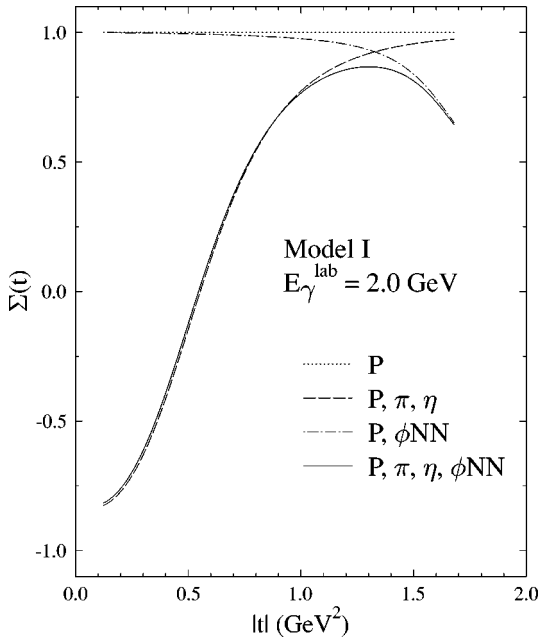

FIG. 9. Model I photon polarization asymmetry (Σ) t dependence near threshold, showing results from different amplitude combinations.

fractive contribution at $E_\gamma^{\rm lab}=2.0$ GeV and for small $|t|$ is nearly an order of magnitude smaller than the contribution from η exchange. The cross section t dependence in all models show strong sensitivity to the ϕNN couplings and all models prefer a very small effective tensor coupling, $g^T_{\phi NN}=g^V_{\phi NN}\kappa^T_\phi$. Model I incorporates the smallest ϕNN couplings (consistent with OZI suppression) yet it produces a sizable contribution as $|t|$ increases. Models II(a) and II(b) (Figs. 5 and 6, respectively) show a significant improvement compared to the behavior of the low energy data with increasing $|t|$, even though moderately small ϕNN couplings (consistent with OZI suppression) are required. We note the general trend of all models for increasing and sizable effects from all nondiffractive amplitudes as energy approaches threshold and increasing with $|t|$. From this behavior we infer the possibility that experiments looking for two-gluon interference signatures (e.g., dip features) at large $|t|$ [29]

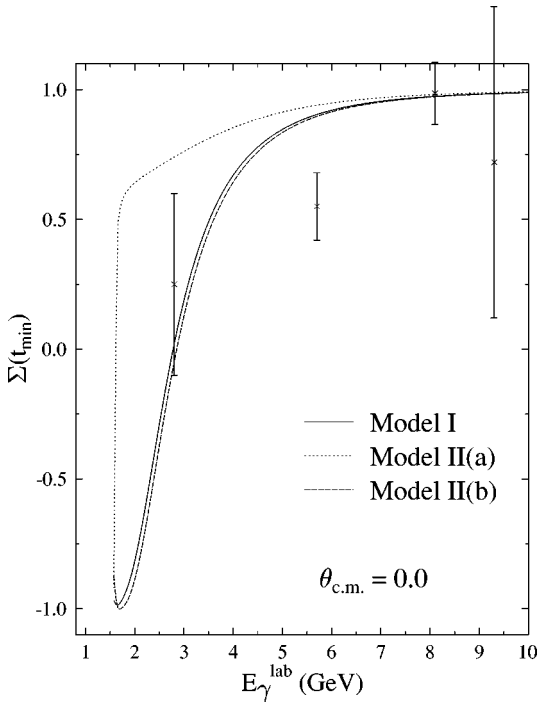

FIG. 8. Threshold energy dependence of models I, II(a), and II(b) photon polarization asymmetry (Σ) at $t_{\rm min}$. The data is a compilation of points with $t\sim t_{\rm min}$ from references in [41].

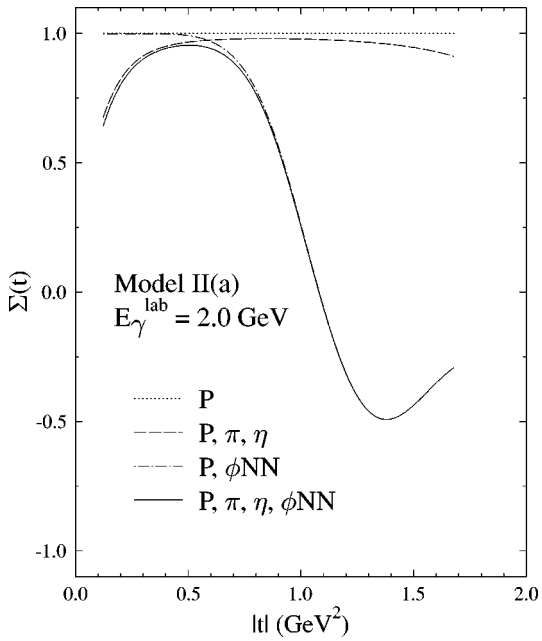

FIG. 10. Model II(a) photon polarization asymmetry (Σ) t dependence near threshold, showing results from different amplitude combinations.

may get ''washed out'' from anomalous backgrounds associated with ϕ production from OZI evading ϕNN couplings and/or strangeness knockout mechanisms (depending on actual magnitude of OZI evading amplitudes and proximity to ϕ threshold energy).

We caution here that the extracted values for the ηNN (and to a lesser degree ϕNN) couplings in models I and II(b) are quite sensitive to the hadronic cutoff parameter λ, whereas in model II(a) the couplings are relatively insensitive to the cutoff. For example, if we increase the cutoff parameter to $\lambda = 0.7$ GeV, then the ηNN couplings of models I and II(b) become suppressed by a factor of approximately 1/3 [consistent with the value found in model II(a)], and the optimal ϕNN couplings also reflect some suppression (although much less than the η couplings). We stress that the hadronic ϕNN and ηNN couplings that we extract in this analysis are only representative values which reflect our model assumptions, and should not be considered as a precise determination of their actual values. We are satisfied with demonstrating sensitivity to these couplings to encourage new experiments, which will undoubtedly lead to further theoretical refinements.

We demonstrate the consistency of models I, II(a), and II(b) with data at higher energy ($E_\gamma^{\rm lab} = 6.45$ GeV) in Fig. 7. All models presented become purely diffractive at high energy. In Fig. 8 we plot the photon polarization asymmetry (Σ) energy dependence at $t_{\rm min}$ for all models. The deviation from unity toward negative values near threshold is primarily a consequence of the η exchange amplitude, although the very steep dependence of model II(a) exactly at threshold arises from the ϕNN contribution. Figures 9, 10, and 11 show the t dependence of Σ near threshold ($E_\gamma^{\rm lab} = 2.0$ GeV) for models I, II(a), and II(b), respectively. Each model produces very different behavior for the Σ t dependence, which supports our claim that precision measurements using linearly polarized photons with full angular coverage can be quite decisive in constraining the dynamics of threshold ϕ photoproduciton. Another persistent feature in Figs. 9–11 is that all models show Σ near threshold to be dominated by η exchange at $t_{\rm min}$ and the ϕNN amplitude at $t_{\rm max}$.

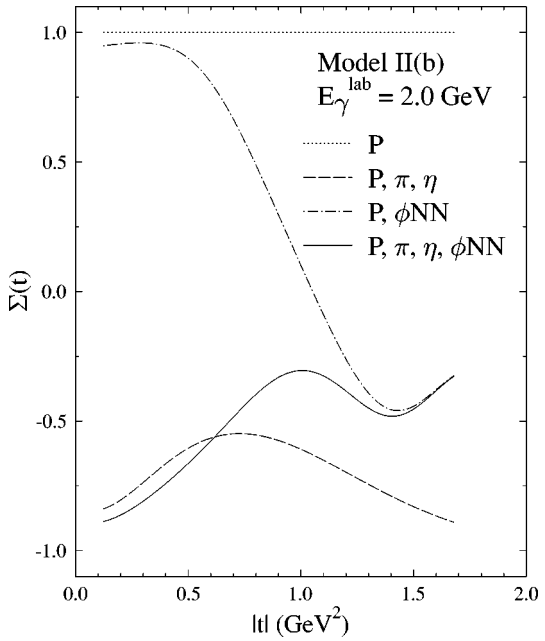

FIG. 11. Model II(b) photon polarization asymmetry (Σ) t dependence near threshold, showing results from different amplitude combinations.

VII. CONCLUSIONS

We have shown that ϕ photoproduction near threshold is sensitive to nondiffractive amplitudes involving OZI evading ϕNN coupling to the proton, especially for $|t| > |t_{\rm min}|$. Measurements using linearly polarized photons and detecting the full angular distribution of the $\phi \to K^+K^-$ decay will be able to extract 9 independent polarization density matrix elements. The linear photon polarization can be achieved at Jefferson Lab through an approved coherent bremsstrahlung facility [42,43] or a proposed laser Compton backscattering facility [44], and will permit a separation of natural and unnatural parity amplitude contributions. The threshold energy region is interesting because the enhanced sensitivity to nondiffractive amplitudes permit measurements to constrain and/or extract uncertain and theoretically important hadronic constants (such as the ηNN, ϕNN couplings and Pomeron Regge trajectory parameters), and establish the threshold energy dependence of the diffractive Pomeron exchange amplitude. Although not explicitly calculated in this study, new ϕ photoproduction measurements near threshold may also provide the opportunity to extract $f_0(980)$ and $a_0(980)$ scalar meson cross sections through S-P wave interference distortions of the K^+K^- angular distribution, and investigate possible novel physics such as enhanced production from candidate strange-exotic X-baryon resonances.

ACKNOWLEDGMENTS

The author appreciates helpful discussions with Phil Cole, Rolf Ent, Dave Tedeschi, Adam Szczepaniak, and Nathan Isgur. This work was supported by NSF Grant No. HRD-9633750.

[1] J. Reifenrother *et al.*, The ASTERIX Collaboration, Phys. Lett. B **267**, 299 (1991); M. A. Faessler *et al.*, The Crystal Barrel Collaboration, Phys. At. Nucl. **57**, 1693 (1994); V. G. Ableev *et al.*, The OBELIX Collaboration, *ibid.* **57**, 1716 (1994); Phys. Lett. B **334**, 237 (1994).

[2] S. Okubo, Phys. Lett. **5**, 165 (1963); G. Zweig, CERN Report No. 8419/TH412, 1964; I. Iizuka, Prog. Theor. Phys. **38**, 21 (1966).

[3] Y. Lu, B. S. Zou, and M. P. Locher, Z. Phys. A **345**, 207 (1993).

[4] M. P. Locher, Y. Lu, and B. S. Zou, Z. Phys. A **347**, 281 (1994).

[5] D. Buzatu and F. M. Lev, Phys. Lett. B **329**, 143 (1994).

[6] V. Mull, K. Holinde, and J. Speth, Phys. Lett. B **334**, 295 (1994).

[7] M. P. Locher and Yang Lu, Z. Phys. A **351**, 83 (1995).

[8] A. V. Anisovich and E. Klempt, Z. Phys. A **354**, 197 (1995).
[9] V. E. Markushin and M. P. Locher, hep-ph/9707491; Report No. PSI-PR-97-17.
[10] Harry J. Lipkin, Nucl. Phys. **B244**, 147 (1984).
[11] P. Geiger and N. Isgur, Phys. Rev. Lett. **67**, 1066 (1991); Report No. CEBAF-TH-96-08.
[12] J. Ellis, M. Karliner, E. E. Kharzeev, and M. G. Sapozhnikov, Phys. Lett. B **353**, 319 (1995).
[13] D. Buzatu and F. M. Lev, Phys. Rev. C **51**, R2893 (1995).
[14] C. B. Dover and P. M. Fishbane, Phys. Rev. Lett. **62**, 2917 (1989).
[15] J. Ellis, E. Gabathuler, and M. Karliner, Phys. Lett. B **217**, 173 (1989).
[16] J. K. Storrow, Phys. Lett. B **230**, 124 (1989).
[17] J. Ashman *et al.*, EMC Collaboration, Phys. Lett. B **206**, 364 (1988).
[18] L. A. Ahrens *et al.*, Phys. Rev. D **35**, 785 (1987).
[19] J. F. Donoghue and C. R. Nappi, Phys. Lett. **168B**, 105 (1986); J. Gasser, H. Leutwyler, and M. E. Sainio, Phys. Lett. B **253**, 252 (1991).
[20] E. M. Henley, G. Krein, S. J. Pollock, and A. G. Williams, Phys. Lett. B **269**, 31 (1991); E. M. Henley, G. Krein, and A. G. Williams, *ibid.* **281**, 178 (1992).
[21] A. I. Titov, S. N. Yang, and Y. Oh, Nucl. Phys. **A618**, 259 (1997); nucl-th/9612059, 1996; Phys. Rev. Lett. **79**, 1634 (1997); nucl-th/9702015, 1997.
[22] Derek B. Leinweber, Nucl. Phys. **A585**, 341c (1995).
[23] G. Hohler *et al.*, Nucl. Phys. **B114**, 505 (1976).
[24] S. Dubnicka, Nuovo Cimento A **100**, 1 (1988).
[25] R. L. Jaffe, Phys. Lett. B **229**, 275 (1989).
[26] M. Gari and W. Krumpelmann, Phys. Lett. B **274**, 159 (1992).
[27] R. A. Williams, S. Krewald, and K. Linen, Phys. Rev. C **51**, 566 (1995).
[28] Ulf-G. Meißner, V. Mull, J. Speth, and J. W. Van Orden, Report No. JLAB-THY-97-02, hep-ph/9701296.
[29] J. M. Laget *et al.*, Jefferson Lab experiment E-93-031.
[30] M. A. Pichowsky, Ph.D. thesis, University of Pittsburg, 1996.
[31] T. Hatsuda, Nucl. Phys. **B329**, 376 (1990).
[32] C. Bennhold, L. Tiator, and S. S. Kamalov, Nucl. Phys. **A585**, 313c (1995).
[33] L. G. Landsberg, Spokesperson, SPHINX Collaboration, *PANIC96*, Williamsburg, VA, 1996 (unpublished).
[34] S. V. Golovkin *et al.*, Z. Phys. C **68**, 585 (1995).
[35] N. Isgur (private communication).
[36] K. Schilling, P. Seyboth, and G. Wolf, Nucl. Phys. **B15**, 397 (1970).
[37] D. P. Barber *et al.*, Z. Phys. C **12**, 1 (1982).
[38] P. D. B. Collins, *An Introduction to Regge Theory and High Energy Physics* (Cambridge University Press, Cambridge, 1977).
[39] Z. Li, Phys. Rev. C **52**, 1648 (1995).
[40] D. Lu, R. H. Landau, and S. C. Phatak, Phys. Rev. C **52**, 1662 (1995).
[41] G. McClellan *et al.*, Phys. Rev. Lett. **26**, 1597 (1971); H. J. Besch *et al.*, Nucl. Phys. **B70**, 257 (1974); D. P. Barber *et al.*, Phys. Lett. **79B**, 150 (1978); H.-J. Behrend *et al.*, Nucl. Phys. **B144**, 22 (1978).
[42] P. Cole (private communication).
[43] D. J. Tedeschi *et al.*, Proposal to Jefferson Lab PAC12, 1997 (unpublished).
[44] R. Ent *et al.*, CEBAF Letter of Intent, 1994 (unpublished).